Journal of Paleontology, page 1 of 12

0022-3360/24/1937-2337
doi: 10.1017/jpa.2024.18

JOURNAL OF PALEONTOLOGY
A PUBLICATION OF THE Paleontological SOCIETY

Virtual taphonomy of trilobite heads: understanding compressive deformation using 3D modeling and rigid body simulation

Jikhan Jung,[1,2]* Tae-Yoon S. Park,[1,2] and Nigel C. Hughes[3]

[1]Division of Earth Sciences, Korea Polar Research Institute, 26 Songdomirae-ro, Yeonsu-gu, 21990 Incheon, Republic of Korea <jikhanjung@kopri.re.kr> <typark@kopri.re.kr>
[2]Polar Science, University of Science and Technology, Daejeon 34113, Republic of Korea
[3]Department of Earth and Planetary Sciences, University of California, Riverside, California 92521, USA <nigel.hughes@ucr.edu>

Non-technical Summary.—After fossils form, their original shape can become distorted, which makes it hard for scientists to figure out what these ancient creatures really looked like in life. This problem affects many aspects of the study of ancient life forms, including understanding how such organisms moved or how they were related to each other. Scientists try to overcome these distortions by figuring out how the fossils got bent out of shape in the first place. Although we know a bit about how the Earth's tectonic movement can distort fossils, we are still learning about the details of how pressure affects the shape of organisms as they turn into fossils. In this study, we used three-dimensional computer simulations to see how fossils of ancient sea creatures called trilobites might have changed shape when they were buried and distorted over time. We found that trilobites on flat ground stayed more true to their original shape than those on uneven ground. Also, the way a trilobite was positioned when it was fossilized—whether it was right-side up or flipped over—made a big difference in how much its shape changed. This research helps us form a better picture of what trilobites and other ancient animals looked like in real life.

Abstract.—Shape deformation during fossilization can prevent accurate reconstruction of an organism's form during life, hampering areas of paleontology ranging from functional morphology to systematics. Retrodeformation attempts to restore the original shape of deformed fossil specimens and requires an adequate knowledge of the deformation process. Although tectonic processes and retrodeformation are relatively well understood, research on quantifying the effect of compressive deformation on fossil morphology is scant. Here we investigate the factors that can cause changes in the shape of fossil specimens during compressive deformation. Three-dimensional (3D) models of trilobite cranidia/cephala are subjected to simulated deposition and compaction using rigid body simulation and scaling features of the open-source 3D software Blender. The variation in pitch and roll angle is lowest on flat surfaces, intermediate on tilted surfaces, and highest on irregular surfaces. These trends are reflected in the morphological differences captured by principal component scores in geometric morphometric analyses using landmarks. In addition, the different shapes of trilobite cranidia/cephala according to their systematic affinity influence the degree of angular variation, which in turn affects their posture —normal or inverted. Inverted cranidia/cephala show greater morphological variability than those with normal postures.

Introduction

Paleontological research relies heavily on morphological information derived from ancient organisms. Fossil shape is the primary information utilized in areas such as morphometrics, functional morphology, phylogenetics, and taxonomy. However in the process of fossilization, morphology can be deformed with factors such as the rigidity of the organism's skeleton, the characteristics of the surrounding sediments, the orientation of the fossils at the time of burial, and the pressure exerted on the matrix (Ferguson, 1963; Campbell and Kauffman, 1969; Briggs and Williams, 1981; Cooper, 1990).

The fossilization process can be divided into several steps, starting with burial. Once a benthic or free-swimming organism dies, its body parts, either articulated or disarticulated, settle onto the seafloor, which can have a flat, tilted, or irregular surface. The orientation (roll, pitch, and yaw angles) of the organism's remains are influenced by the seafloor's topography and by the subsequent sedimentation process. As the matrix compacts due to the loading of overlying sediment during burial, compressive force is exerted on the remains of the organism, which operates at different angles on fossils buried in different orientations (Ferguson, 1963; Campbell and Kauffman, 1969). After lithification, tectonic forces can act on rocks enclosing the fossils. The stress and strain caused by these forces can result in dilation, compression, and shear of the fossil specimens. The degree of tectonic deformation can vary from one specimen to another, or even within different parts

*Corresponding author.

of the same specimen, making it challenging to accurately restore the original shapes of fossil organisms (Ramsay and Huber, 1983; Cooper, 1990; Hughes and Jell, 1992). To account for such postmortem variation, it is important to understand the particular processes of deformation that occur during and after fossilization. Researchers interested in fossil deformation have mostly focused on the tectonic processes and retrodeformation, whereas there have been only a few, if any, studies that have quantitatively investigated compressive deformation and its effects on fossil morphology (Hughes and Rushton, 1990; Webster and Hughes, 1999).

In the nineteenth century, Haughton (1856) and Harker (1885) drew attention to slaty cleavage and the distortion of fossils. Methods to retrodeform distorted fossils were suggested and formulated in the twentieth century (e.g., Lake, 1943). Ramsay and Huber (1983) established a textbook approach using the strain ellipse in their structural geology book, whereas simpler and easier approaches were frequently used by paleontologists (Wellman, 1962; Sdzuy, 1966; Cooper, 1970, 1990). In addition to the mathematical understanding and restoration of deformed fossils, ways to utilize technological advances were also explored, such as the Analog Video Reshaper (Appleby and Jones, 1976), Tilt Correction feature of scanning electron microscope (Veltkamp and Donovan, 1984), user-defined enlargement/reduction ratios of x- and y-axes in laser copiers after calculating the strain ratio (Rushton and Smith, 1993), and computer-aided restoration (Hughes and Rushton, 1990) with an early use of a commercial graphics package to do this being that of Hughes and Jell (1992). In the late 1970s and early 1980s, Doveton (1979) and Briggs and Williams (1981) showed a keen interest in restoring the three-dimensional (3D) shape of organisms from flattened fossils. One of the most notable advances in technology was the widespread availability of computerized tomography (CT) scanning during the 1990s. Vertebrate paleontologists and paleoanthropologists began utilizing CT scanning and 3D models (Zollikofer et al., 1995, 1998, 2005; Ponce de León and Zollikofer, 1999; Ogihara et al., 2006; Molnar et al., 2012; Schlager et al., 2018) (see Lautenschlager, 2016 for a comprehensive review). Engineering-oriented approaches, e.g., Finite Element Analysis, have also been incorporated into the study of fossil deformation (Rayfield et al., 2007; Polly et al., 2016). The rise of geometric morphometrics has provided another useful tool for researchers (Bookstein, 1978, 1989; Zelditch et al., 2004). With all of these methods and tools at our disposal, now it is possible to examine the fossilization process and related shape changes in greater detail.

In this study, we conducted a virtual taphonomic experiment using three kinds of differently shaped trilobite head parts—cranidia of *Estaingia* Pocock, 1964 and *Taebaeksaukia* Lee and Choi, 2011, and cephala of *Phacops* Emmrich, 1839—to gain a methodical understanding of the depositional processes on three surface types. By determining the possible range of the pitch and roll angles of cranidia/cephala under known parameters, the variation in the morphology after compressive deformation can be understood. Our aim is to provide a better picture of fossil compressional shape changes occurring prior to any subsequent tectonic deformation.

Theoretical background

Compressive deformation.—During fossilization, the remains of the organism are typically subjected to vertical pressure from the weight of sediment above. The pressure applied to the fossils and the way that deformation progresses can vary depending on the composition of the sediment and the nature of the remains. Ferguson (1963) demonstrated that brachiopod shells preserved in shale were compressed to approximately one-third of their original thickness when compared to nondeformed specimens, and that the sediment surrounding the fossil was compressed to approximately one-sixth of its original thickness. The alteration of fossil morphology due to compression also depends on the angle at which the fossil was deposited on the seafloor. For instance, Boulter (1968) investigated compression fossils of lycopod sporophyll and described how the orientation of the sporophyll in the sediment affects the final appearance of the fossils. Campbell and Kauffman (1969) demonstrated that the length ratio between parts of the head of the trilobite *Olenellus* Hall, 1862 after compaction can differ from the original ratio depending on the angle at which the specimen is placed on the seafloor. Hughes and Rushton (1990) also observed a difference in the shape of the trilobite pygidium due to its orientation (normal or flipped). Harris (1974) conducted experiments with an elastic ball to understand how compression affects the shape of spherical pollen grains.

The pressure exerted during the lithification process can also cause cracks in the rigid exoskeleton. Webster and Hughes (1999) studied the cephalon of *Olenellus* and *Nephrolenellus* Palmer and Repina, 1993 to analyze the pattern of cracks and to demonstrate how cracks develop with and without a hypostome underneath the cephalon. Using morphometric analysis with landmarks, they showed that trilobite cephala preserved in shale have large displacements at the landmarks on both corners in the posterolateral region compared to specimens preserved in limestone. They raised the possibility that this pattern is due to cracks caused by vertical pressure during the lithification process, rather than by intraspecific variation.

Once the trilobite sclerite, e.g., a cranidium or a cephalon, settles on the seafloor, it forms a specific angle with the seafloor surface. This angle can be subdivided into the roll angle (angle of rotation along the anteroposterior axis), the pitch angle (angle of rotation along the lateral axis that runs across the left and right sides of the head part), and the yaw angle (angle of rotation along the vertical axis; in the case of trilobite head part, the dorsoventral axis, and the compass direction to which the sagittal axis is aligned) (Fig. 1). It can be important to consider the yaw angle when investigating the effects of water currents on taphonomy, but to understand the morphology affected by compression, only the pitch and roll angles are relevant.

When the trilobite is alive and places its prone body parallel to the seafloor, as most benthic trilobites would have done, the posture of the head part at that moment can be considered the 'normal posture,' with both the roll and pitch angles equal to zero. In most benthic trilobites, this 'normal posture' would correspond to the posture in which the anterior and lateral margin of the cephalon lies flat on the seafloor surface. Once the organism died and its exoskeleton disarticulated, the cranidium or cephalon

https://doi.org/10.1017/jpa.2024.18 Published online by Cambridge University Press

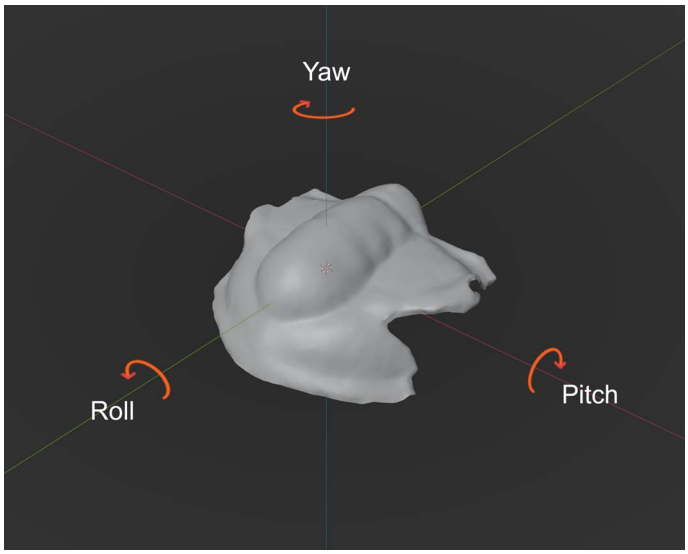

Figure 1. Pitch, roll, and yaw angles in a trilobite cranidium.

could have become detached from the body and settled separately on the seafloor. If the cranidium or cephalon rotated along either its anteroposterior or transverse axes, for example, because the cranidium without the librigena could not support itself and tipped backward on the surface or tumbled around due to a water current or other animals' activities, the roll and pitch angles would have values other than zero. In such cases, compression during fossilization could alter the shape of the fossil trilobite head depending on the roll and pitch angles (Fig. 2). This effect becomes more noticeable as the convexity of the trilobite head increases, as seen in the case of *Phacops* (Fig. 2.2, 2.5) compared to those of *Estaingia* (Fig. 2.1, 2.4) or *Taebaeksaukia* (Fig. 2.3, 2.6).

Consider a hypothetical case involving a group of trilobites belonging to the same species characterized by a prominently convex cranidium. This assemblage consists of numerous cranidia, divided evenly, wherein half of them are positioned with a pitch angle of 25° and the other half with a pitch angle of −25°. Such distribution would create a bimodal distribution. This scenario could be plausible if the cranidium's shape positions the center of gravity near where the anterior branch of the facial suture meets the anterior margin of the cranidium in lateral view. In that case, the point where the facial suture meets the anterior margin of the cranidium might serve as a pivot point, leading to the cranidium settling on the ocean floor with an almost equal probability of resting at either a 25° or −25° pitch angle. In cases of considerable compaction, the observed bimodal distribution could imply the existence of two distinct types of trilobites (Fig. 2).

Nedin and Jenkins (1999) identified species within *Estaingia* and *Xystridura* Whitehouse, 1936 to form an ancestor-descendant lineage with one of the main differences between the two genera as the length of the preglabellar field. However, as shown in the previous example, the proportions of the preglabellar field can vary with changes in pitch angle. To ensure that such variation in the ratio of two lengths is not a taphonomic artifact, it is necessary to understand the causes and effects of taphonomic deformation processes.

Tectonic deformation.—Another source of deformation in fossils is tectonic forces. Once the lithification process is complete, the rock layers within which the fossils are contained can be subject to movement and stress caused by Earth's tectonic movements. Folding and faulting can cause distortion or even destruction of fossils.

With an increasing number of fossil specimens accessible in digital format, retrodeformation has become a popular method for addressing the problem of deformation. Various retrodeformation methods have been proposed and utilized, with most focusing on finding a strain ellipse and then restoring the

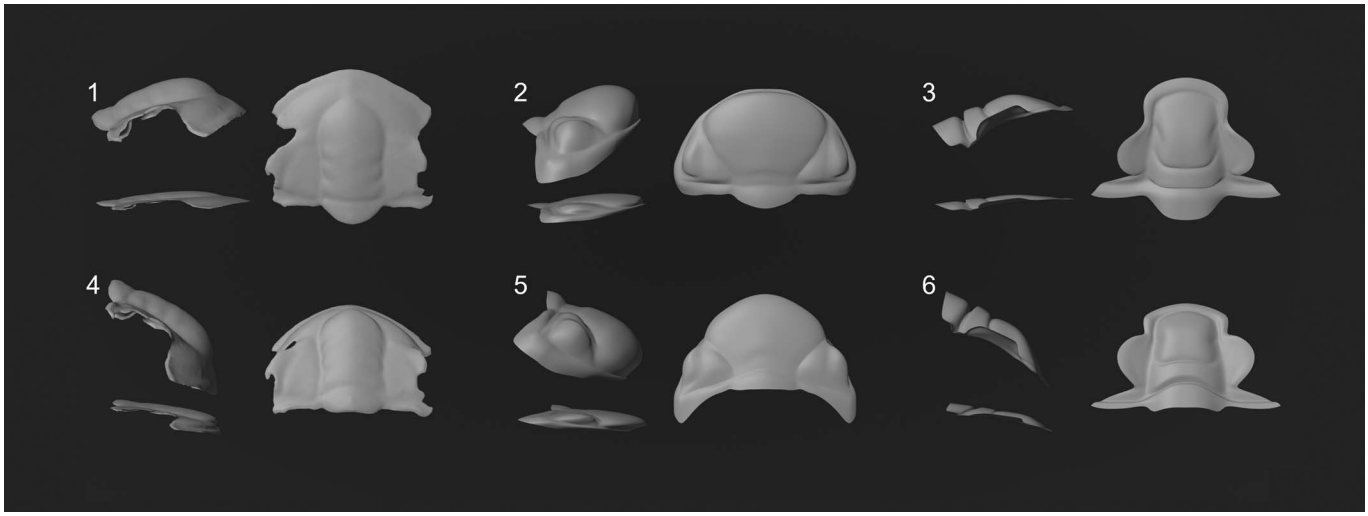

Figure 2. Effects of pitch angle variation combined with compressive deformation: (**1**) *Estaingia* cranidium at +25° pitch angle, lateral views before and after compressive deformation, and dorsal view postdeformation; (**2**) *Phacops* cephalon at +25° pitch angle, lateral views before and after deformation, and dorsal view postdeformation; (**3**) *Taebaeksaukia* cranidium at +25° pitch angle, lateral views before and after deformation, and dorsal view postdeformation; (**4**) *Estaingia* cranidium at −25° pitch angle, lateral views before and after deformation, and dorsal view postdeformation; (**5**) *Phacops* cephalon at −25° pitch angle, lateral views before and after deformation, and dorsal view postdeformation; (**6**) *Taebaeksaukia* cranidium at −25° pitch angle, lateral views before and after deformation, and dorsal view postdeformation.

https://doi.org/10.1017/jpa.2024.18 Published online by Cambridge University Press

original shape accordingly. Different approaches have been taken to find the strain ellipse or the axis of maximum extension. Bilateral symmetry of the organism is then utilized to determine the amount of extension or contraction required to restore the original shape. In most cases, it is difficult or impossible to restore the original size and shape of fossil organisms, so restoration of the original shape or bilateral symmetry is often considered a satisfactory result (Ramsay and Huber, 1983; Cooper, 1990; Hughes and Rushton, 1990; Hughes and Jell, 1992; Rushton and Smith, 1993; Srivastava and Shah, 2006; but see Angielczyk and Sheets, 2007).

Wellman's (1962) method for finding the strain ellipse caused by tectonic deformation is relatively simple and does not require complicated mathematical calculations. This method requires at least two specimens, each with two originally perpendicular axes defined. Points of intersection of the projections of the same axes in each of the two deformed specimens allow for identification of the strain ellipse that is common to both.

If there is no rock slab with multiple deformed specimens of bilaterally symmetrical organisms, one can try to find the axis of maximum extension, which is typically indicated by parallel lineations on the surface of the rock slab (Rushton and Smith, 1993). The bilateral symmetry of the fossil specimen can be restored by dilating/extending along that axis or the axis perpendicular to it (Ramsay and Huber, 1983; Cooper, 1990; Hughes and Rushton, 1990; Hughes and Jell, 1992; Rushton and Smith, 1993; Srivastava and Shah, 2006).

Motani (2007) developed a technique in which a 3D surface model of a deformed specimen is manipulated using computer graphics software, and retrodeformed by removing the effects of deformation. The deformation is assumed to be caused by the compression of the specimen along a single axis, and the amount of compression is estimated by finding the minimum cross-sectional area of the specimen.

Angielczyk and Sheets (2007) introduced a method that involves simulating the tectonic deformation of a turtle plastron and assessing whether retrodeformation can preserve the biological signals that are present in nondeformed datasets. To do this, they prepared an actual dataset of turtle plastron and also created an artificial dataset of the same object based on a hatchling and an adult specimen from the actual dataset, using a linear model to interpolate between those specimens, with a small amount of Gaussian noise added. They applied a strain matrix to the datasets to simulate tectonic deformation. After deformation, all of the landmark coordinates were superimposed using the Procrustes superimposition method. The study conducted a retrodeformation analysis using three different methods to remove the effects of simulated tectonic deformation. These methods included reflecting and averaging landmarks based on bilateral symmetry, retrodeformation based on Principal Component Analysis (PCA), and removal of the affine transformation (commonly assumed to represent deformation in earlier retrodeformations). Geometric morphometric analysis of the deformed and retrodeformed specimens revealed that none of the retrodeformation methods were able to completely remove the effects of simulated tectonic deformation. Specifically, the removal of the affine transformation consistently produced worse results than the other two methods, indicating that this approach should not be used if the goal is to retrieve biological signals from deformed fossil specimens. Nonetheless, the study demonstrated that simulation is a useful way to understand the nature of tectonic deformation and its effects on biological signals.

Materials and methods

3D models.—Three 3D models—two cranidia and a cephalon (Fig. 3)—were assembled to reflect the disparate morphologies of trilobite heads among three different trilobite genera. The first one was a limestone-preserved cranidium of *Estaingia* that showed a relatively consistent width throughout. The *Estaingia* cranidium was 3D scanned using a SkyScan 1273 micro-CT scanner. The resulting image stack was then segmented in the open-source software 3D Slicer and exported as an .STL file for import into the open-source 3D software Blender (https://www.blender.org), where post-processing was conducted. The limestone matrix was removed from the 3D model to isolate the cranidium. The initial model consisted of approximately 400,000 faces, but was simplified to 9,000 faces to improve computational performance without significantly altering the overall shape of the cranidium. The second model was a *Phacops* cephalon, in which there was no dorsal facial suture. This model of the *Phacops* cephalon was created manually in Blender based on pictures from Clarkson

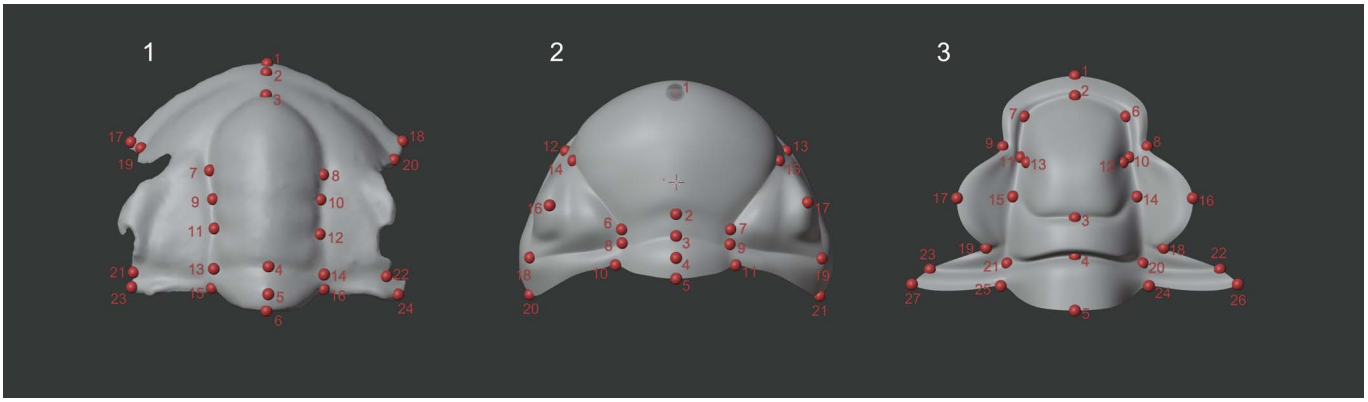

Figure 3. Location of cranidial/cephalic landmarks selected for morphometric analysis of shape deformation during taphonomy: (**1**) 24 cranidial landmarks of *Estaingia*; (**2**) 27 cephalic landmarks of *Phacops*; (**3**) 21 cranidial landmarks of *Taebaeksaukia*.

https://doi.org/10.1017/jpa.2024.18 Published online by Cambridge University Press

(1966) and a 3D scanned model of *Phacops* downloaded from Sketchfab (https://sketchfab.com). The third model was a cranidium of *Taebaeksaukia* characterized by its broader posterior end compared to the anterior end. This *Taebaeksaukia* cranidium was also manually modelled in Blender based on photographs from Lee and Choi (2011).

Taphonomy simulation.—To explore the influence of the distributions of roll and pitch angles on the preserved morphology of the trilobite head part during the fossilization process, a taphonomy simulation was conducted using 3D models of the cranidia/cephala placed above the seafloor with random roll and pitch angles assigned. The simulation began by letting the model fall freely under the influence of gravity, observing the range of possible postures that it could be achieved when settling on the seafloor before becoming buried. The simulation was performed using Blender's rigid body simulation feature, in which the model was set as an active rigid body and the plane representing the seafloor was set as a passive rigid body. This allowed the 3D models of the cranidium/cephalon to interact with the plane, settle on it with stable roll and pitch angles, and collide without deformation during the deposition simulation. The purpose of this simulation was to observe the distribution of possible roll and pitch angles that can occur during the fossilization process.

When the experimental conditions remained constant, the trilobite head parts consistently settled on the seafloor at the same roll and pitch angles, regardless of how many times the experiment was repeated. Our goal was to determine the whole range and possible distribution of roll and pitch angles when multiple cranidia/cephala are fossilized. To achieve this, we began with a trilobite head that was set up as a rigid body and used a Python script to replicate the model 100 times. The duplicated cranidia/cephala were spaced at a suitable distance from each other to avoid interference during the simulation. Each replicated model was randomly rotated along the lateral axis (pitch angle) and anteroposterior axis (roll angle). In the simulation settings of Blender, the collision shape of the cranidium/cephalon was set to 'Convex hull' to reduce computational complexity. The plane representing the seafloor was set to 'Mesh' so that its tilted or irregular surface could interact with the cranidium/cephalon and have an effect on the simulation.

Data collection.—Trilobite head parts that settled on the seafloor are oriented in different directions depending on the slope and curvature of the seafloor. To assess the distribution of the pitch and roll angles of the cranidia/cephala for each trilobite genus, we extracted the pitch and roll angles of each trilobite head part with respect to the seafloor using a Python script and stored the result in a text file with tab-delimited format. The cranidium/cephalon's final posture, whether normal or inverted, was determined based on the pitch and roll angles. A posture was categorized as normal if the model settled on the surface with its dorsal (convex) side facing upward and as inverted if it settled with the ventral (concave) side up. Regarding the specific angles, a posture was considered normal if the final orientation exhibited a deviation of <45° from a 0° roll or pitch angle. Conversely, an orientation was deemed inverted if it showed a deviation of <45° from a 180° roll or pitch angle. The specimen was classified as normal when both roll and pitch angles indicated an inverted position.

Compressive deformation.—After collecting pitch and roll angles for the 100 cranidia/cephala, they were subjected to compressive deformation simulation. This step simulates the effect of compaction prior to lithification and is achieved by scaling the z-axis to 30% of its original length, an estimate derived from the example of brachiopod fossilized in shale illustrated by Campbell and Kauffman (1969).

Geometric morphometrics.—Geometric morphometrics, especially when employing 3D landmarks, is one of the best ways to capture and explore morphological changes in organisms, as shown by Hopkins and Pearson (2016). To quantitatively measure the cranidium/cephalon's morphology and its changes, we assigned 24 landmarks to *Estaingia,* 21 to *Phacops*, and 27 to *Taebaeksaukia* (Fig. 3, Appendix). Each landmark was placed on a vertex of the 3D model, and the index of the corresponding vertex was recorded. After the compressive deformation (meaning that the coordinates of the landmarks were moved from their original position relative to other landmarks), the x-, y-, and z-coordinates of the landmarks were extracted to generate a resulting dataset. A Python script was employed to iterate over the recoded vertex indices to obtain the corresponding landmarks' x-, y-, and z-coordinates from the deformed 3D model. The dataset was saved as a .TPS file, a widely used file format in geometric morphometrics. For actual analyses, we used Modan2, a comprehensive morphometric software (available at https://github.com/jikhanjung/Modan2). The .TPS files containing landmark data were loaded into Modan2, where further details were added. This additional information included the classification of the surface type, identified as either flat, tilted, or irregular, and the posture of the cranidium, specifying whether it was in a normal or inverted position. A single dataset was generated from one surface type for each trilobite genus. Three datasets, each representing a different surface type, were merged to form a consolidated dataset for each genus. The landmark data from each genus dataset were translated, scaled, and rotated using the Procrustes superimposition method. Principal component analyses were then performed to examine the shape variation.

Statistical analyses.—To investigate whether the shape changes according to the surface types as well as to the postures of the head parts were statistically significant, we performed PerMANOVA and multivariate dispersion test on the landmark data in PAST, the paleontological statistics software version 4.08 (Hammer et al., 2001).

In a typical morphometric study, organisms are divided into groups based on their characteristics. The most commonly used method to measure the differences among groups is MANOVA or a variant of MANOVA, e.g., PerMANOVA (Hammer and Harper, 2008; Anderson, 2017). These statistical methods show the difference between the groups in terms of their multivariate means. However, the ranges of variation between the surface types and postures are more focused in this study, i.e., how

https://doi.org/10.1017/jpa.2024.18 Published online by Cambridge University Press

different surface types create variation in the settled cranidia/cephala shapes, and how posture affects the variation. In this respect, the standard deviation of principal component scores or the multivariate dispersion is more relevant to this study than the multivariate mean used in MANOVA variants.

Results

Distribution of the pitch and roll angles.—The x-axis indicates the pitch angle and the y-axis indicates the roll angle in nine scatter plots of the distribution of the pitch and roll angles of cranidia/cephala from three trilobite genera on three surface types (Fig. 4). Cranidia/cephala that are inverted around the transverse axis (~180° of pitch angle) are plotted on the bottom right of the graph and cranidia that inverted around the anteroposterior axis (~180° of roll angle) are plotted on the top left of the graph. In the lower left corner are the head parts without inversion, and in the upper right corner are those that have inverted around both the lateral and anteroposterior axes, resulting in a dorsal-up posture. In other words, there are four clusters of roll and pitch angle combinations, two diagonally arranged clusters at the upper left and lower right corners that represent inverted cranidia/cephala, and the rest are the normal ones.

In the scatterplots of the flat surface (Fig. 4.1, 4.2, 4.3), the variations in pitch and roll angles are the smallest. With respect to the posture of the specimen, normal cranidia/cephala show little variation in both angles, whereas inverted specimens show noticeable variation in their distribution, in the pitch angle for *Estaingia*, and in the roll angle for *Phacops*, but not for *Taebaeksaukia*.

In the second row (Fig. 4.4, 4.5, 4.6), the tilted surface produced scatterplots with more variation in the pitch and roll angles. A peculiarity of the *Phacops* plot on the tilted surface (Fig. 4.5) is that there are two clusters of points that are not seen in other plots, at ~120° and 310° of pitch angle. Investigation showed that these are the cephala in an upright posture, with their posterior ends in contact with the surface and their anterior

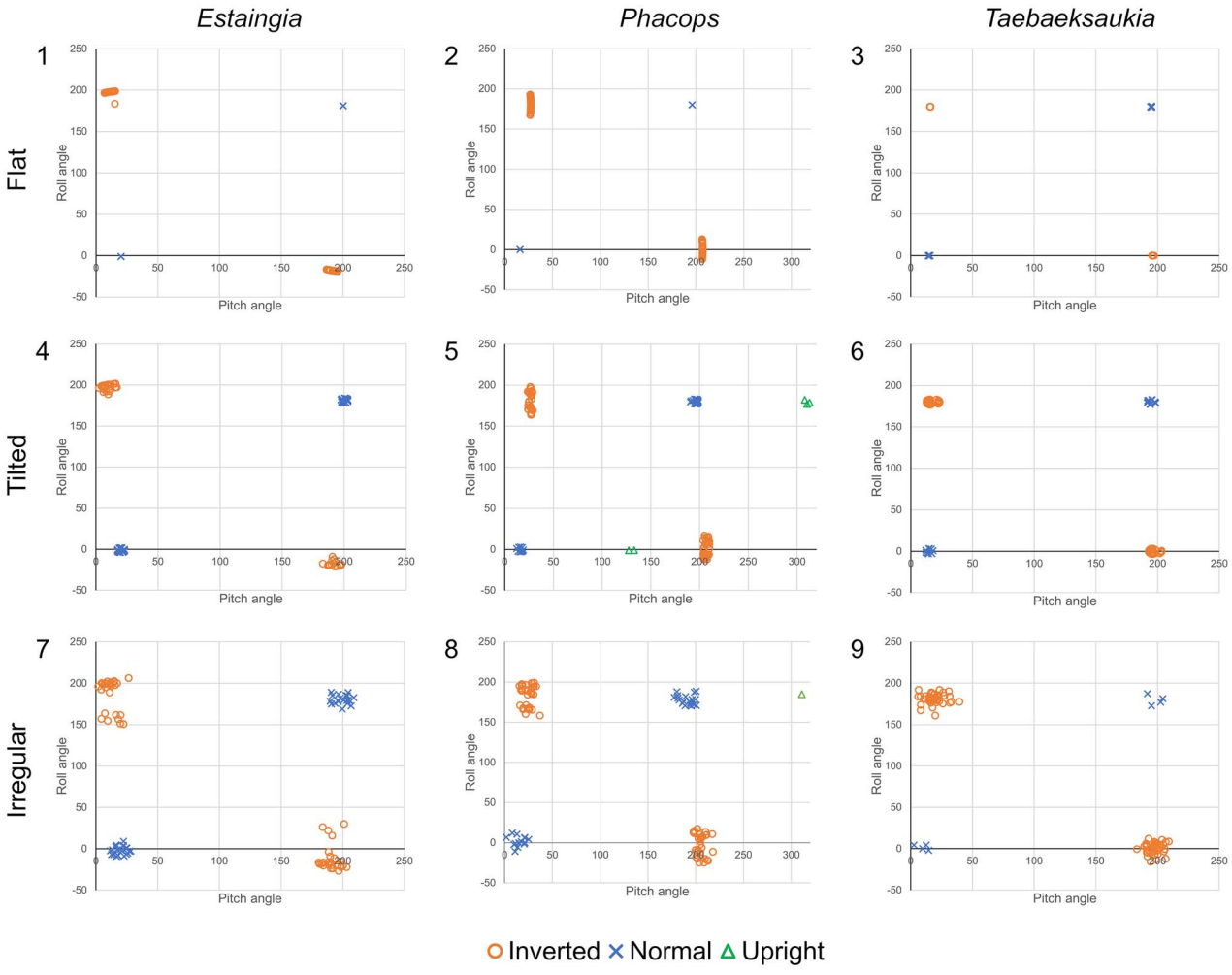

Figure 4. Bivariate plots of the distribution of pitch and roll angles of three trilobite genera on three surface types: (**1**) *Estaingia* on a flat surface; (**2**) *Phacops* on a flat surface; (**3**) *Taebaeksaukia* on a flat surface; (**4**) *Estaingia* on a tilted surface; (**5**) *Phacops* on a tilted surface; (**6**) *Taebaeksaukia* on a tilted surface; (**7**) *Estaingia* on an irregular surface; (**8**) *Phacops* on an irregular surface; (**9**) *Taebaeksaukia* on an irregular surface.

https://doi.org/10.1017/jpa.2024.18 Published online by Cambridge University Press

ends pointing upward. Similar data points can be found in the *Phacops* plot of the irregular surface, but in smaller numbers.

Of the three surface types, irregular ones show the most variation in the roll and pitch angles of trilobite head parts (Fig. 4.7, 4.8, 4.9).

Settled specimens can have three postures, i.e., normal, inverted, and upright. In *Estaingia*, the ratio of normal specimens and inverted specimens was ∼1:1, whereas in *Phacops* this ratio became 1:2 and in *Taebaeksaukia* 1:4. Upright specimens were found only in *Phacops* from tilted and irregular surfaces (Table 1).

Geometric morphometric analyses.—Figure 5 summarizes the results of geometric morphometric analyses. The first row shows the PCA result by surface type: flat surface (blue circles), tilted surface (green squares), and irregular surface (black triangles). From the *Phacops* dataset, however, the specimens with upright postures were excluded from the geometric morphometric analysis, being outliers that would distort the morphospace and hamper detailed investigation of the effects of compressive deformation. The morphological variation of trilobite head after compressive deformation along PC1 and PC2 is shown in the matrices, with nine configurations displayed for each genus (Fig. 6). These configurations combine the three principal component scores —minimum, average, and maximum—on PC1 with the corresponding three scores on PC2, thereby providing a comprehensive view of the morphological variation.

Most of the shape variation can be explained by the first two principal components (90.0% for *Estaingia*, 99.5% for *Phacops*, 98.2% for *Taebaeksaukia*) (Table 2) and thus the PCA results are shown as two-dimensional scatter plots using PC1 and PC2 (Fig. 5).

In the PCA results, the *Estaingia* cranidia from the flat surface (blue circles) grouped into three clusters (Fig. 5.1). The normal specimens group around the PC1 value of 0.17 and the rest are the inverted specimens (Fig. 5.4), most lined up along the PC1 value of -0.2 and a single specimen at the coordinate (0.073, 0.009). The data from the tilted surface occupies a larger area in the plot than those from the flat surface. Normal specimens form a circle centered on the normal cluster of the flat surface. Inverted specimens are more widely distributed on the negative side of PC1. Irregular surface-generated data points (black triangles) appear all around the plot, indicating the widest variation in their shapes. Shape changes along PC1 predominantly reflect the roll angle, indicating whether the cranidium tilted to the left or right when it settled. The variation along PC2, observable from the same dorsal perspective, relates to the pitch angle, affecting the perceived elongation or shortening of the cranidium along the organism's anteroposterior axis (Fig. 6.1).

As for *Phacops*, normal specimens from the flat surface clustered at the coordinates (0.023, 0.045) in PC1 and PC2 axes (Fig. 5.2, 5.5), with very little shape variation, similar to *Estaingia* from the flat surface. Inverted specimens from the flat surface form a line between PC1 values of -0.08 and 0. As in *Estaingia*, data from the tilted surface are distributed similarly to those from the flat surface, but spread more widely. Normal specimens from the tilted surface are shown in a line close to the normal specimen cluster from the flat surface. Inverted specimens from tilted surface are aligned with the normal specimens in the flat surface, with a wider distribution (Fig. 5.2, 5.5). Specimens from the irregular surface are scattered throughout the plot, resembling an arrowhead pointing to the left. In *Phacops*, the most noticeable shape change is the elongation or shortening of the cephalon (Fig. 6.2) rather than the roll angle-related shape change that is prominent in *Estaingia* (Fig. 6.1). As we move from the average to the maximum values on both PC1 and PC2, the cephalon with a normal posture appears progressively shorter (Figs. 5.5, 6.2). Conversely, when moving toward the minimum value of PC2, the cephalon with an inverted posture elongates. This pattern underscores the distinct morphological responses of the cephalon to variations in these principal components.

Compared to *Estaingia* and *Phacops*, *Taebaeksaukia* showed relatively narrower distribution of pitch and roll angles on flat and tilted surfaces (Fig. 5.3, 5.6). Normal specimens from the flat surface clustered at the coordinates of (0.01, 0.007) in PC1 and PC2 axes. Inverted specimens from the flat surface scattered around the normal specimens and their PC1 values ranged from -0.015 to 0.015 (Fig. 5.3, 5.6). Normal specimens from the tilted surface distributed around the normal specimens from the flat surface and their PC1 values ranged 0.005–0.023. As in other genera, specimens from the irregular surface show the greatest variation in *Taebaeksaukia*, with PC1 and PC2 values ranging at least twice as much as those from the flat or tilted surfaces (Fig. 5.3). The morphological changes of *Taebaeksaukia*'s cranidium, like in *Phacops*, exhibits elongation and shortening with variations in PC1 and PC2, although to a more subtle degree (Fig. 6.3).

Variation in the ranges of PC1 and PC2 values is reflected in their statistical properties, e.g., variance or standard deviation (Table 3). In most cases, the standard deviation value tends to increase within the same genus as the surface type changes from flat to tilted, and from tilted to irregular. Also, specimens with inverted postures tend to have higher standard deviations than those with normal postures.

Statistical tests.—As shown in the previous section, for all three trilobite genera, the standard deviation of PC scores tended to increase as the surface type changed from flat to tilted, and from tilted to irregular. This was confirmed by the multivariate dispersion test on the PC values of the superimposed landmark data. Figure 7 summarizes multivariate dispersion data in six box plots. In the upper row (Fig. 7.1, 7.2, 7.3), the boxplots show that the flat surface resulted in the lowest level of dispersion, the tilted surface resulted in an intermediate level, and the irregular surface resulted in the highest level of

Table 1. Number of specimens in each posture and surface type after taphonomy simulation.

	Estaingia		*Phacops*			*Taebaeksaukia*	
	Normal	Inverted	Normal	Inverted	Upright	Normal	Inverted
Flat	44	56	28	72	0	29	71
Tilted	51	49	29	66	5	23	77
Irregular	36	64	33	66	1	8	92
Sum	131	169	90	204	6	60	240

https://doi.org/10.1017/jpa.2024.18 Published online by Cambridge University Press

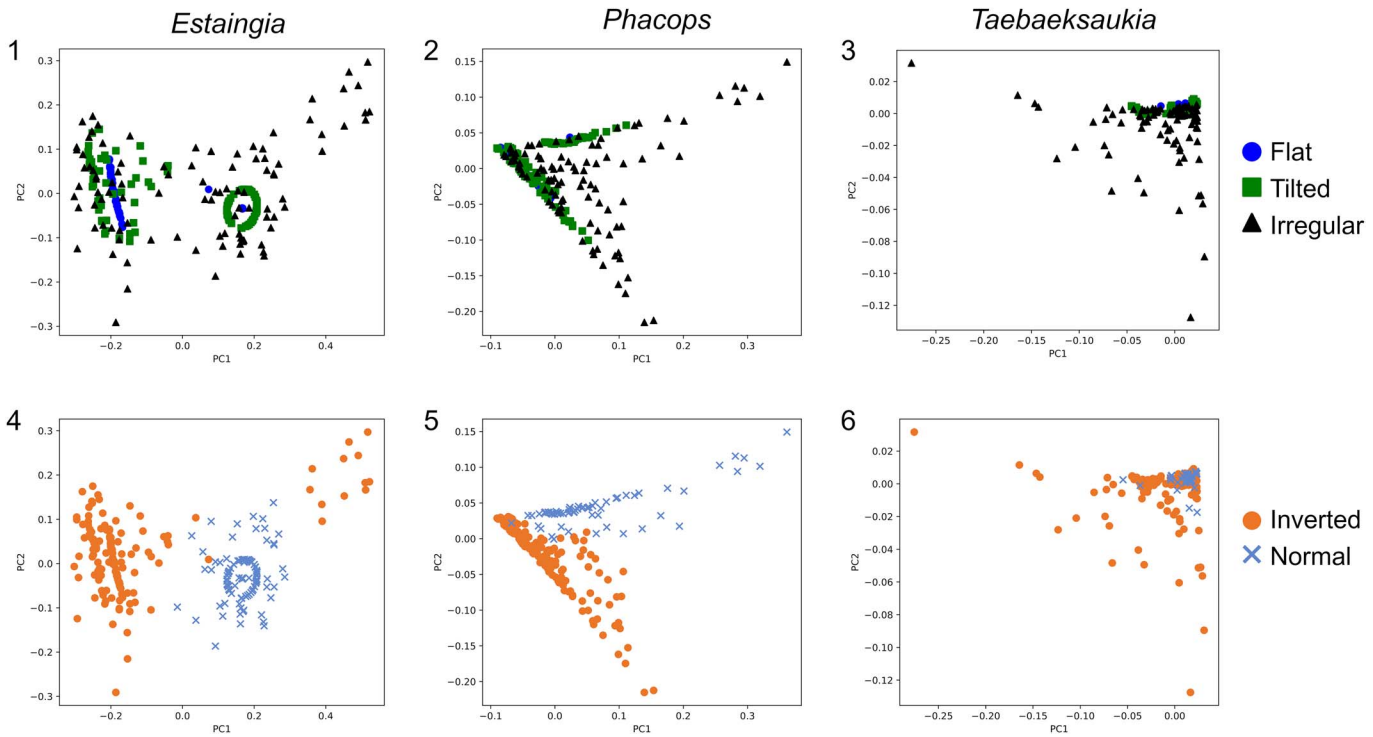

Figure 5. PCA results of three trilobite genera on three surface types: (**1**) *Estaingia* with symbols differentiated by the surface type; (**2**) *Phacops* with symbols differentiated by the surface type; (**3**) *Taebaeksaukia* with symbols differentiated by the surface type; (**4**) *Estaingia* with symbols differentiating their cranidial posture; (**5**) *Phacops* with symbols differentiating their cranidial posture; (**6**) *Taebaeksaukia* with symbols differentiating their cranidial posture.

dispersion in each genus. In the lower row (Fig. 7.4, 7.5, 7.6), normally oriented specimens showed lower dispersion in *Estaingia* and *Taebaeksaukia*, but not in *Phacops*.

Statistical tests of multivariate dispersion yielded Bonferroni-corrected p-values of < 0.01 in most cases (Table 4). In summary, the changes in multivariate dispersion according to surface type and cranidial posture are statistically significant except in two cases, between flat surface and tilted surface as well as between inverted specimens and normal specimens in *Phacops*.

Discussion

Estaingia cranidia on the flat surface with normal posture showed practically no variation in their roll and pitch angles. On the other hand, inverted *Estaingia* cranidia on the flat surface showed a larger variation in pitch angle of ~8–9°. This means that on a flat surface, the inverted *Estaingia* cranidia could have more than one stable position in which to settle, because stability can be achieved in several postures as different parts of gently curved convex surface of the glabella and either the

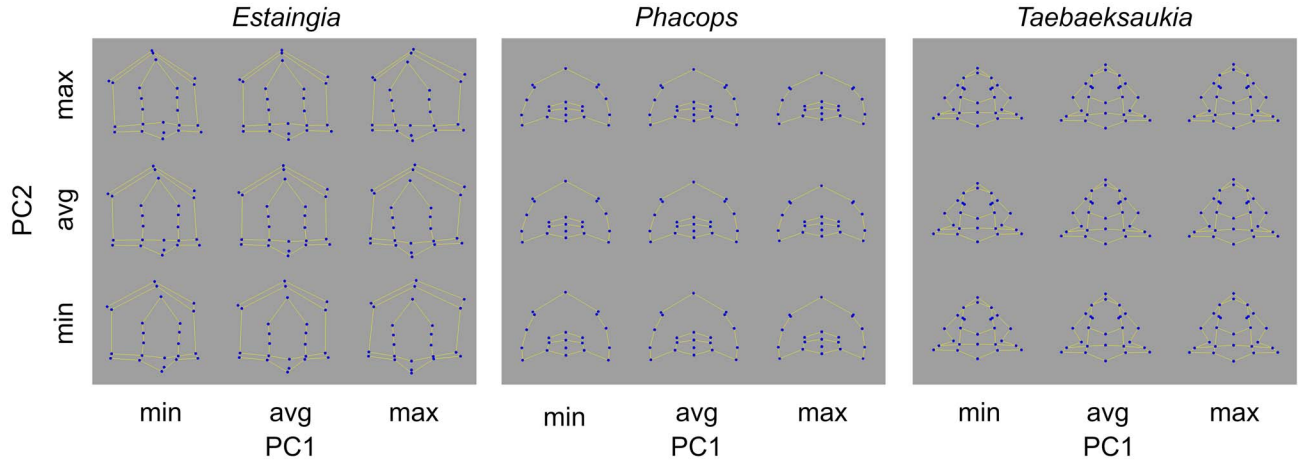

Figure 6. PCA morphospace visualization: (**1**) *Estaingia* cranidium shape variations; (**2**) *Phacops* cephalon shape variations; (**3**) *Taebaeksaukia* cranidium shape variations. Each set depicts the morphological changes across the minimum, average, and maximum values of principal component axes 1 and 2.

https://doi.org/10.1017/jpa.2024.18 Published online by Cambridge University Press

Table 2. Morphological variation after taphonomy simulation and compressive deformation explained by first four principal component scores.

	PC1	PC2	PC3	PC4
Estaingia	79.282	10.708	7.118	2.810
Phacops	67.989	31.484	0.001	0.000
Taebaeksaukia	82.911	15.337	0.005	0.002

Table 3. Standard deviation of the principal component scores according to the surface types and postures.

Genus			PC1	PC2
Estaingia	Surface	Flat	0.178	0.038
		Tilted	0.194	0.057
		Irregular	0.244	0.112
	Posture	Normal	0.046	0.049
		Inverted	0.181	0.087
Phacops	Surface	Flat	0.040	0.027
		Tilted	0.043	0.038
		Irregular	0.092	0.068
	Posture	Normal	0.083	0.023
		Inverted	0.052	0.045
Taebaeksaukia	Surface	Flat	0.003	0.001
		Tilted	0.020	0.002
		Irregular	0.048	0.021
	Posture	Normal	0.013	0.005
		Inverted	0.034	0.015

Table 4. Bonferroni-corrected p-values from the multivariate dispersion tests.

	versus		*Estaingia*	*Phacops*	*Taebaeksaukia*
Surface	Flat	Tilted	0.0024	0.2595	0.0003
	Flat	Irregular	0.0003	0.0003	0.0003
	Tilted	Irregular	0.0003	0.0003	0.0003
Posture	Normal	Inverted	0.0001	0.3484	0.0006

left or right palpebral lobe contact with the surface. Such variation can be magnified as the shape of the surface departs increasingly from a flat, horizontal plane. On a uniformly tilted surface, cranidia with normal posture formed a circle on the scatter plot because, with enough specimens, there are specimens with their anteroposterior axes pointing in every direction on the tilted surface. As the surface is uniformly tilted, a specimen with maximal pitch angle has zero roll angle (anteroposterior axis perpendicular to the plane's strike direction), and as the pitch angle decreases, the roll angle increases accordingly, so that a specimen with maximum roll angle (anteroposterior axis parallel to the strike direction) has the average pitch angle. For the irregular surface, the pitch and roll angles of the cranidia are more spread out than for the previous two surface types. In the inverted specimens, each cluster clearly has two smaller clusters. These clusters correspond to specimens that are inverted and tilted to the left (right palpebral lobe in contact with the surface) and specimens that are inverted and tilted to the right (left palpebral lobe in contact with the surface). After compressive deformation, these inverted specimens show asymmetry because the compressive force is applied obliquely to the lateral axis of the cranidium due to the roll angle.

In *Phacops* and *Taebaeksaukia*, the general pattern of variation in the pitch and roll angles was similar to that observed in *Estaingia*, starting with the lowest variation on the flat surface and increasing as the surface type changes to tilted then to irregular. *Taebaeksaukia* specimens on the flat and tilted

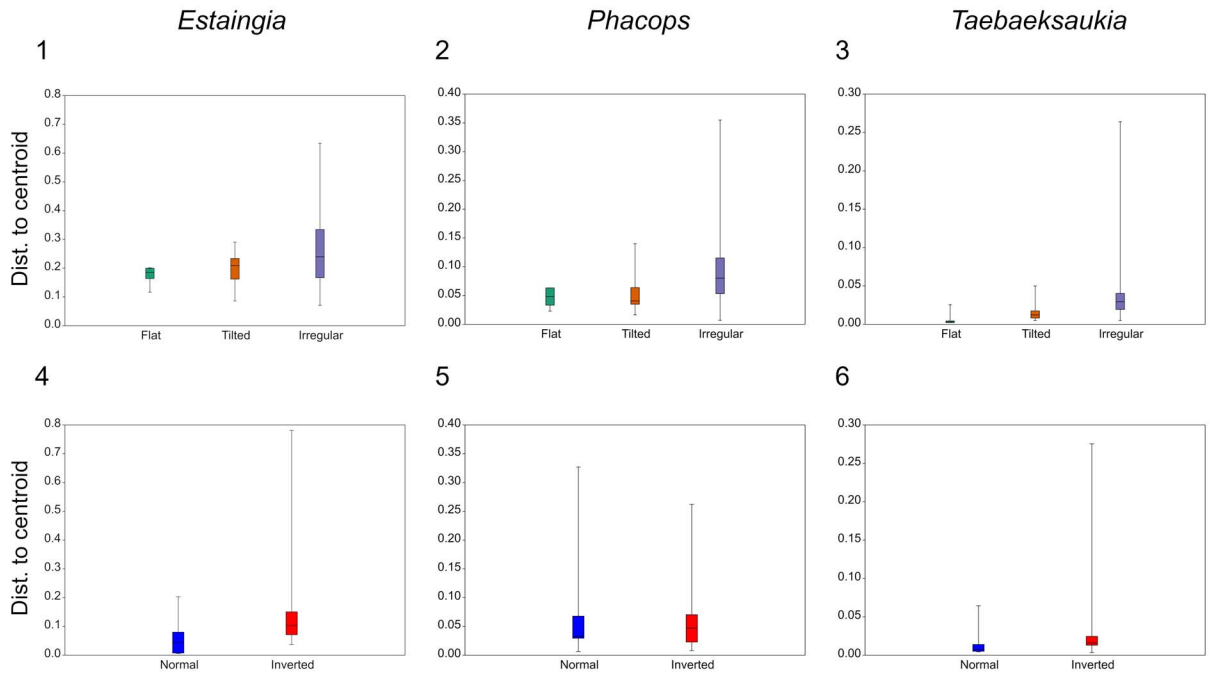

Figure 7. Multivariate dispersion test results, summarized as box plots: (**1**) multivariate dispersion of *Estaingia* PC scores by surface type; (**2**) multivariate dispersion of *Phacops* PC scores by surface type; (**3**) multivariate dispersion of *Taebaeksaukia* PC scores by surface type; (**4**) multivariate dispersion of *Estaingia* PC scores by cranidial posture; (**5**) multivariate dispersion of *Phacops* PC scores by cephalic posture; (**6**) multivariate dispersion of *Taebaeksaukia* PC scores by cranidial posture.

https://doi.org/10.1017/jpa.2024.18 Published online by Cambridge University Press

surfaces showed little variance in the roll and pitch angles. It is likely that the shape of cranidium affected this result because the posterior border of *Taebaeksaukia* is the widest part of the cranidium, with the anterior end of the cranidium plus the left and right ends of the posterior border acting as a fairly stable, triangular support on the flat or tilted surface.

In contrast to *Estaingia* and *Taebaeksaukia*, *Phacops* has a fused dorsal suture and its head part is thus a cephalon. As a result, the lateral ends of the *Phacops* cephalon are gently curved whereas those of *Estaingia* or *Taebaeksaukia* show large indentations into which their free cheeks fit. Due to the nonseparated free cheeks and the absence of genal spines, the *Phacops* cephalon is dorsoventrally thicker than in the other two trilobites. This might be the reason why the upright posture is achieved only in *Phacops*, because the occipital ring and both posterolateral ends of cephalon could have acted as a tripod when it settled.

A significant proportion of the morphological variation in trilobite cranidia/cephala (at least 90%) is encapsulated within the first two principal components (Table 2). This implies that the bivariate plots captured most of the shape variation across all three genera (Fig. 5). In the cases of *Estaingia* and *Taebaeksaukia*, specimens in inverted positions exhibit a broader distribution along PC1 and PC2, translating into greater variance (Fig. 7). In Figures 7.4–7.6, a considerable portion of morphological variation, particularly in *Estaingia* and *Taebaeksaukia*, can be attributed to specimens in inverted positions.

There are, however, limitations of the simulation method used in this study. For example, in the simulation settings, we assumed that the seafloor acted as a rigid body, but shale or carbonate rock at the time of deposition was unlikely to have provided a hard surface. With a soft or semisoft surface, part of the cranidium/cephalon could have penetrated the sediment resulting in an orientation that would not be possible if it were deposited under the influences of gravity, water current, and the seafloor surface alone.

When a trilobite's exoskeletal component is released above the seafloor in water, its descent is influenced by its interaction with the water. This phenomenon was explored by Hesselbo (1987) using cranidial and pygidial models in a water tank experiment to observe their settling behavior. The distinct shapes of the cranidium and pygidium resulted in different behaviors during descent, suggesting that their interaction with the water largely predetermined the final resting posture of these exoskeletal parts. Hesselbo (1987) reported that in still water, most cranidia fell in an inverted posture, whereas most pygidia fell in a normal posture. Because his experiment dealt with only one genus, *Dikelocephalus* Owen, 1852, it is hard to compare his results directly to our results. Although the proportion of normal to inverted cranidia in *Taebaeksaukia* on irregular surfaces (8% normal, 92% inverted) resembles Hesselbo's (1987) findings (~10% normal in still water), this similarity might be coincidental. In Hesselbo's (1987) study, the *Dikelocephalus* models physically interacted with the water, whereas our simulations could not account for the dynamic interaction between the head parts and the water during descent. Addressing this aspect would require a comprehensive computational fluid dynamics simulation.

Similarly, the orientation of the cranidium/cephalon is finalized when it settled on the seafloor in our models. In reality, the sclerite can be pushed around by other organisms or currents, or sediments can be deposited under, around, and above the cranidium, thus stabilizing its position. This is especially true for inverted specimens. In most such cases, these specimens have the glabella and one fixed cheek in contact with the seafloor surface, whereas the other cheek would be projecting obliquely upward. In the landmark analysis, these specimens showed deformed landmarks along the glabellar lateral margin being displaced, forming two roughly parallel lines curved in the same direction, which originally would be expected to form a mirror image of the opposing side of the glabella due to bilateral symmetry.

Compressive and tectonic deformations pose other questions for this simulation study. When the deposited cranidium and its surrounding sediments are compacted due to pressure from the overlying sediments and/or tectonic pressure, the cranidium can become deformed based on the interaction between the material properties of the cranidium (calcite in this case) and the characteristics of the sediments around it. Depending on how they interact with each other and also with water that exists in the space between sediments, the deformation can depart from simple compression.

Concluding remarks

This study suggests that during the depositional processes, both the shape of the seafloor surface and the shapes of the sclerites being deposited, in this case trilobite cranidia/cephala, affect the pitch and roll angles preserved by the fossils. The variation in pitch and roll angle tends to be lowest on flat surfaces, intermediate on tilted surfaces, and highest on irregular surfaces. This tendency is reflected in the morphological variation captured by the first two principal component scores of landmark-based geometric morphometric analyses. The different shapes of trilobite cranidia/cephala also have an effect on the degree of variation in the pitch and roll angles, and subsequently whether they have normal, upright, or inverted postures during fossilization. Cranidia/cephala with inverted postures tend to have a higher variability in their morphology compared to those with normal postures.

Acknowledgments

This work was supported by a Korea Polar Research Institute (KOPRI) grant funded by the Ministry of Oceans and Fisheries (KOPRI project no. PE24050). NCH was supported by U.S. National Science Foundation grant EAR-1849963. We also greatly appreciate constructive comments from two anonymous reviewers.

Declaration of competing interests

The authors declare that they have no known competing interests or personal relationships that could have appeared to influence the work reported in this paper.

References

Anderson, M.J., 2017, Permutational Multivariate Analysis of Variance (PERMANOVA), *in* Kenett, R.S., Longford, N.T., Piegorsch, W.W., and Ruggeri, F., eds., Wiley StatsRef: Statistics Reference Online (first edition): Hoboken, New Jersey, John Wiley and Sons, p. 1–15.

https://doi.org/10.1017/jpa.2024.18 Published online by Cambridge University Press

Angielczyk, K.D., and Sheets, H.D., 2007, Investigation of simulated tectonic deformation in fossils using geometric morphometrics: Paleobiology, v. 33, p. 125–148, https://doi.org/10.1666/06007.1.
Appleby, R.M., and Jones, G.L., 1976, The analogue video Reshaper—a new tool for palaeontologists: Palaeontology, v. 19, p. 565–586.
Bookstein, F.L., 1978, The Measurement of Biological Shape and Shape Change: Berlin, Springer Berlin Heidelberg, 191 p.
Bookstein, F.L., 1989, Principal warps: thin-plate splines and the decomposition of deformations: IEEE Transactions on Pattern Analysis and Machine Intelligence, v. 11, p. 567–585.
Boulter, M.C., 1968, A species of compressed lycopod sporophyll from the Upper Coal Measures of Somerset: Palaeontology, v. 11, p. 445–457.
Briggs, D.E.G., and Williams, S.H., 1981, The restoration of flattened fossils: Lethaia, v. 14, p. 157–164.
Campbell, L., and Kauffman, M.E., 1969, *Olenellus* fauna of the Kinzers Formation, southeastern Pennsylvania: Proceedings of the Pennsylvania Academy of Science, v. 43, p. 172–176.
Clarkson, E.N.K., 1966, The life attitude of the Silurian trilobite *Phacops mushéni* Salter 1864: Scottish Journal of Geology, v. 2, p. 76–83.
Cooper, R.A., 1970, Tectonic distortion of a syntype of *Isograptus forcipiformis latus* Ruedemann: Journal of Paleontology, v. 44, p. 980–983.
Cooper, R.A., 1990, Interpretation of tectonically deformed fossils: New Zealand Journal of Geology and Geophysics, v. 33, p. 321–332.
Doveton, J.H., 1979, Numerical methods for the reconstruction of fossil material in three dimensions: Geological Magazine, v. 116, p. 215–226.
Emmrich, H. F., 1839, De Trilobitis; Dissertatio Petrefactologica: Berlin, Nietackianis, 56 p.
Ferguson, L., 1963, Estimation of the compaction factor of a shale from distorted brachiopod shells: SEPM Journal of Sedimentary Research, v. 33, p. 796–798.
Hall, J., 1862, Supplementary note to the thirteenth report of the Regents of the State Cabinet, *in* Fifteenth Annual Report of the New York State Cabinet for Natural History: Albany, New York, p. 113–119.
Hammer, Ø., and Harper, D.A.T., 2008, Paleontological Data Analysis: Hoboken, New Jersey, John Wiley & Sons, 368 p.
Hammer, Ø., Harper, D.A.T., and Ryan, P.D., 2001, PAST: Paleontological statistics software package for education and data analysis: Palaeontologia Electronica, v. 4, https://palaeo-electronica.org/2001_1/past/issue1_01.htm.
Harker, A., 1885, On slaty cleavage and allied rock-structures, with special reference to the mechanical theories of their origin: Report, British Association for the Advancement of Science, 55th Meeting, Aberdeen, Scotland: London, John Murray, p. 813–852.
Harris, T.M., 1974, *Williamsoniella lignieri*: its pollen and the compression of spherical pollen grains: Palaeontology, v. 17, p. 125–148.
Haughton, S., 1856, On slaty cleavage, and the distortion of fossils: The London, Edinburgh, and Dublin Philosophical Magazine and Journal of Science, v. 12, p. 409–421.
Hesselbo, S.P., 1987, The biostratinomy of *Dikelocephalus* sclerites: implications for the use of trilobite attitude data: Palaios, v. 2, p. 605–608.
Hopkins, M.J., and Pearson, J.K., 2016, Non-linear ontogenetic shape change in *Cryptolithus tesselatus* (Trilobita) using three-dimensional geometric morphometrics: Palaeontologia Electronica, v. 19, p. 1–54, https://doi.org/10.26879/665.
Hughes, N.C., and Jell, P.A., 1992, A statistical/computer-graphic technique for assessing variation in tectonically deformed fossils and its application to Cambrian trilobites from Kashmir: Lethaia, v. 25, p. 317–330.
Hughes, N.C., and Rushton, A.W.A., 1990, Computer-aided restoration of a late Cambrian ceratopygid trilobite from Wales, and its phylogenetic implications: Palaeontology, v. 33, p. 429–445.
Lake, P., 1943, Restoration of the original form of distorted specimens: Geological Magazine, v. 80, p. 139–147.
Lautenschlager, S., 2016, Reconstructing the past: methods and techniques for the digital restoration of fossils: Royal Society Open Science, v. 3, n. 160342, https://doi.org/10.1098/rsos.160342.
Lee, S.-B., and Choi, D.K., 2011, Dikelocephalid trilobites from the Eosaukia fauna (upper Furongian) of the Taebaek Group, Korea: Journal of Paleontology, v. 85, p. 279–297, https://doi.org/10.1666/10-034.1.
Molnar, J., Pierce, S., Clack, J., and Hutchinson, J., 2012, Idealized landmark-based geometric reconstructions of poorly preserved fossil material: a case study of an early tetrapod vertebra: Palaeontologia Electronica, v. 15, n. 15.1.2T, https://doi.org/10.26879/274.
Motani, R., 2007, New technique for retrodeforming tectonically deformed fossils, with an example for ichthyosaurian specimens: Lethaia, v. 30, p. 221–228, https://doi.org/10.1111/j.1502-3931.1997.tb00464.x.
Nedin, C., and Jenkins, R.J.F., 1999, Heterochrony in the Cambrian trilobite *Hsuaspis*: Alcheringa: An Australasian Journal of Palaeontology, v. 23, p. 1–7.
Ogihara, N., Nakatsukasa, M., Nakano, Y., and Ishida, H., 2006, Computerized restoration of nonhomogeneous deformation of a fossil cranium based on bilateral symmetry: American Journal of Physical Anthropology, v. 130, p. 1–9, https://doi.org/10.1002/ajpa.20332.
Owen, D.D., 1852, Report of the Geological Survey of Wisconsin, Iowa and Minnesota: Philadelphia, Lippencott, Grambo, and Company, 638 p.
Palmer, A.R., and Repina, L.N., 1993, Through a glass darkly: taxonomy, phylogeny, and biostratigraphy of the Olenellina: University of Kansas Paleontological Contributions, n. ser., no. 3, 35 p.
Pocock, K.J., 1964, *Estaingia*, a new trilobite genus from the lower Cambrian of South Australia: Palaeontology, v. 7, p. 458–471.
Polly, P.D., Stayton, C.T., Dumont, E.R., Pierce, S.E., Rayfield, E.J., and Angielczyk, K.D., 2016, Combining geometric morphometrics and finite element analysis with evolutionary modeling: towards a synthesis: Journal of Vertebrate Paleontology, v. 36, n. e1111225, https://doi.org/10.1080/02724634.2016.1111225.
Ponce de León, M.S., and Zollikofer, C.P.E., 1999, New evidence from Le Moustier 1: computer-assisted reconstruction and morphometry of the skull: The Anatomical Record, v. 254, p. 474–489.
Ramsay, J.G., and Huber, M.I., 1983, The Techniques of Modern Structural Geology, Volume 1, Strain Analysis: London, Academic Press, 307 p.
Rayfield, E.J., 2007, Finite element analysis and understanding the biomechanics and evolution of living and fossil organisms: Annual Review of Earth and Planetary Sciences, v. 35, p. 541–576, https://doi.org/10.1146/annurev.earth.35.031306.140104.
Rushton, A.W.A., and Smith, M., 1993, Retrodeformation of fossil—a simple technique: Palaeontology, v. 36, p. 927–930.
Schlager, S., Profico, A., Vincenzo, F.D., and Manzi, G., 2018, Retrodeformation of fossil specimens based on 3D bilateral semi-landmarks: implementation in the R package 'Morpho': PLoS ONE, v. 13, n. e0194073, https://doi.org/10.1371/journal.pone.0194073.
Sdzuy, K., 1966, An improved method of analysing distortion in fossils: Palaeontology, v. 9, p. 125–134.
Srivastava, D.C., and Shah, J., 2006, Digital method for strain estimation and retrodeformation of bilaterally symmetric fossils: Geology, v. 34, p. 593–596, https://doi.org/10.1130/G22374.1.
Veltkamp, C.J., and Donovan, S.K., 1984, A scanning electron microscope technique for restoring deformed fossils: Lethaia, v. 17, p. 191–195.
Webster, M., and Hughes, N.C., 1999, Compaction-related deformation in Cambrian olenelloid trilobites and its implications for fossil morphometry: Journal of Paleontology, v. 73, p. 355–371.
Wellman, H.W., 1962, A graphical method for analysing fossil distortion caused by tectonic deformation: Geological Magazine, v. 99, p. 348–352.
Whitehouse, F.W., 1936, The Cambrian faunas of north-eastern Australia, parts 1 and 2: Memoirs of the Queensland Museum, v. 11, p. 59–112.
Zelditch, M., Swiderski, D.L., Sheets, H.D., and Fink, W.L., 2004, Geometric Morphometrics for Biologists: a Primer: Boston, Elsevier Academic Press, 443 p.
Zollikofer, C.P.E., Ponce de León, M.S., Martin, R.D., and Stucki, P., 1995, Neanderthal computer skulls: Nature, v. 375, p. 283–285.
Zollikofer, C.P.E., Ponce de León, M.S., and Martin, R.D., 1998, Computer-assisted paleoanthropology: Evolutionary Anthropology: Issues, News, and Reviews, v. 6, p. 41–54.
Zollikofer, C.P.E., Ponce de León, M.S., Lieberman, D.E., Guy, F., Pilbeam, D., Likius, A., Mackaye, H.T., Vignaud, P., and Brunet, M., 2005, Virtual cranial reconstruction of *Sahelanthropus tchadensis*: Nature, v. 434, p. 755–759, https://doi.org/10.1038/nature03397.

Appendix. Descriptions of landmark locations used in the geometric morphometric analyses of *Estaingia* and *Taebaeksaukia* cranidia, and *Phacops* cephalon.

Estaingia

1. Anteriormost point of cranidium on sagittal axis.
2. Anteriormost point of anterior border furrow on sagittal axis.
3. Anteriormost point of glabellar anterior lobe (L4) on sagittal axis.
4. Midpoint of SO on sagittal axis.
5. Medial node on occipital ring.
6. Midpoint of posterior edge of occipital ring on sagittal axis.
7. Juncture of axial furrow with S3 (left).
8. Juncture of axial furrow with S3 (right).

https://doi.org/10.1017/jpa.2024.18 Published online by Cambridge University Press

9. Juncture of axial furrow with S2 (left).
10. Juncture of axial furrow with S2 (right).
11. Juncture of axial furrow with S1 (left).
12. Juncture of axial furrow with S1 (right).
13. Juncture of axial furrow with SO (left).
14. Juncture of axial furrow with SO (right).
15. Juncture of axial furrow with posterior margin of cephalon (left).
16. Juncture of axial furrow with posterior margin of cephalon (right).
17. Juncture of anterior margin of cranidium and facial suture line (left).
18. Juncture of anterior margin of cranidium and facial suture line (right).
19. Juncture of anterior border furrow and anterior branch of the facial suture (left).
20. Juncture of anterior border furrow and anterior branch of the facial suture (right).
21. Juncture of posterior border furrow and posterior branch of the facial suture (left).
22. Juncture of posterior border furrow and posterior branch of the facial suture (right).
23. Juncture of posterior edge and posterior branch of the facial suture (left).
24. Juncture of posterior edge and posterior branch of the facial suture (right).

Phacops

1. Anteriormost point of anterior border furrow on sagittal axis.
2. Midpoint of S1 on sagittal axis.
3. Midpoint of SO on sagittal axis.
4. Medial node on occipital ring.
5. Midpoint of posterior edge of occipital ring on sagittal axis.
6. Juncture of axial furrow with S1 (left).
7. Juncture of axial furrow with S1 (right).
8. Juncture of axial furrow with SO (left).
9. Juncture of axial furrow with SO (right).
10. Juncture of axial furrow with posterior margin of cephalon (left).
11. Juncture of axial furrow with posterior margin of cephalon (right).
12. Juncture of anterior border furrow and axial furrow (left).
13. Juncture of anterior border furrow and axial furrow (right).
14. Juncture of palpebral lobe and axial furrow (left).
15. Juncture of palpebral lobe and axial furrow (right).
16. Highest point of the eye (left).
17. Highest point of the eye (right).
18. Juncture of posterior border furrow and lateral border furrow (left).
19. Juncture of posterior border furrow and lateral border furrow (right).
20. Juncture of posterior edge and lateral edge (left).
21. Juncture of posterior edge and lateral edge (right).

Taebaeksaukia

1. Anteriormost point of cranidium on sagittal axis.
2. Anteriormost point of anterior border furrow on sagittal axis.
3. Midpoint of S1 on sagittal axis.
4. Midpoint of SO on sagittal axis.
5. Medial node on occipital ring.
6. Juncture of preglabellar furrow and axial furrow (left).
7. Juncture of preglabellar furrow and axial furrow (right).
8. Anteriormost point of palpebral lobe edge (left).
9. Anteriormost point of palpebral lobe edge (right).
10. Juncture of axial furrow with S2 (left).
11. Juncture of axial furrow with S2 (right).
12. Medial end of S2 (left).
13. Medial end of S2 (right).
14. Juncture of axial furrow with S1 (left).
15. Juncture of axial furrow with S1 (right).
16. Widest point of lateral edge of palpebral lobe (left).
17. Widest point of lateral edge of palpebral lobe (right).
18. Posteriormost point of palpebral lobe edge (left).
19. Posteriormost point of palpebral lobe edge (right).
20. Juncture of axial furrow with SO (left).
21. Juncture of axial furrow with SO (right).
22. Juncture of posterior border furrow and posterior branch of the facial suture (left).
23. Juncture of posterior border furrow and posterior branch of the facial suture (right).
24. Juncture of axial furrow with posterior margin of cranidium (left).
25. Juncture of axial furrow with posterior margin of cranidium (right).
26. Juncture of posterior edge and posterior branch of the facial suture (left).
27. Juncture of posterior edge and posterior branch of the facial suture (right).

Accepted: 28 February 2024

https://doi.org/10.1017/jpa.2024.18 Published online by Cambridge University Press